Pseudogap formation above the superconducting dome in iron pnictides

T. Shimojima,[1,2,*] T. Sonobe,[1] W. Malaeb,[3,4] K. Shinada,[1] A. Chainani,[5,6] S. Shin,[2,3,4,5] T. Yoshida,[4,7] S. Ideta,[1] A. Fujimori,[4,7]
H. Kumigashira,[8] K. Ono,[8] Y. Nakashima,[9] H. Anzai,[10] M. Arita,[10] A. Ino,[9] H. Namatame,[10] M. Taniguchi,[9,10]
M. Nakajima,[4,7,11] S. Uchida,[4,7] Y. Tomioka,[4,11] T. Ito,[4,11] K. Kihou,[4,11] C. H. Lee,[4,11] A. Iyo,[4,11] H. Eisaki,[4,11] K. Ohgushi,[3,4]
S. Kasahara,[12,13] T. Terashima,[12] H. Ikeda,[13] T. Shibauchi,[13] Y. Matsuda,[13] and K. Ishizaka[1,2,14]

[1]*Department of Applied Physics, University of Tokyo, Bunkyo, Tokyo 113-8656, Japan*
[2]*JST, CREST, Chiyoda, Tokyo 102-0075, Japan*
[3]*ISSP, University of Tokyo, Kashiwa 277-8581, Japan*
[4]*JST, TRIP, Chiyoda, Tokyo 102-0075, Japan*
[5]*RIKEN SPring-8 Center, Sayo, Hyogo 679-5148, Japan*
[6]*Department of Physics, Tohoku University, Aramaki, Aoba-ku, Sendai 980-8578, Japan*
[7]*Department of Physics, University of Tokyo, Bunkyo, Tokyo 113-0033, Japan*
[8]*KEK, Photon Factory, Tsukuba, Ibaraki 305-0801, Japan*
[9]*Graduate School of Science, Hiroshima University, Higashi-Hiroshima 739-8526, Japan*
[10]*Hiroshima Synchrotron Center, Hiroshima University, Higashi-Hiroshima 739-0046, Japan*
[11]*National Institute of Advanced Industrial Science and Technology, Tsukuba 305-8568, Japan*
[12]*Research Center for Low Temperature and Materials Sciences, Kyoto University, Kyoto 606-8502, Japan*
[13]*Department of Physics, Kyoto University, Kyoto 606-8502, Japan*
[14]*JST, PRESTO, Kawaguchi, Saitama 332-0012, Japan*

The nature of the pseudogap (PG) in high transition temperature (high T_c) superconducting cuprates has been a major issue in condensed matter physics. It is still unclear whether the high T_c superconductivity can be universally associated with the PG formation. Here we provide direct evidence of the existence of the PG phase via angle-resolved photoemission spectroscopy in another family of high T_c superconductor, iron pnictides. Our results reveal a composition-dependent PG formation in the multiband electronic structure of BaFe$_2$(As$_{1-x}$P$_x$)$_2$. The PG develops well above the magnetostructural transition for low x, persists above the nonmagnetic superconducting dome for optimal x, and is destroyed for $x \sim 0.6$, thus showing a notable similarity with cuprates. In addition, the PG formation is accompanied by inequivalent energy shifts in the zx/yz orbitals of iron atoms, indicative of a peculiar iron orbital ordering which breaks the fourfold rotational symmetry.

The pseudogap (PG) observed in the normal state of the high T_c copper oxide superconductors remains a mysterious state of matter.[1–3] It has been attributed to several mechanisms such as a precursor pairing[4–6] and a novel form of spin/charge ordering.[7–9] Nearly a quarter century after the discovery of high T_c superconductivity,[10] the PG phase is still extensively debated in the literature, and no consensus has been reached regarding its origin. In order to gain further insights into the relationship between the high T_c superconductivity and the PG, the exploration of the PG phase in other high T_c superconductors is highly desired.

Iron pnictides[11] are another class of high T_c superconductors, whose typical phase diagram is shown in Fig. 1(a). The parent compound shows stripe-type antiferromagnetic (AF) ordering at T_N accompanying a lattice distortion from tetragonal to orthorhombic structure at T_s.[12] In contrast to the parent cuprate, which is an AF insulator, the parent pnictide is an AF metal. The electronic structure derived from multiple Fe $3d$ orbitals[13] consists typically of disconnected hole and electron Fermi surfaces (FSs), which undergo an electronic reconstruction across T_N and T_s.[14,15] In addition to spin fluctuations derived from the nesting between the disconnected FSs,[16,17] orbital fluctuations are also a candidate for a driving force of electron pairing in iron pnictides.[18,19] The importance of the orbital degrees of freedom in the itinerant ground

states attracted much attention in terms of orbital ordering, defined as an inequivalent electronic occupation of the zx/yz orbitals.[20–22] Intensive researches suggested that iron pnictides can be distinguished from copper oxides based on its orbital multiplicity and itinerant magnetism. It has been, thus, an important issue whether the high T_c iron pnictide family also exhibits a PG phase in common with cuprates.

One of the most intriguing properties of iron pnictides recently reported is their twofold rotational symmetry of various physical properties below $T_{N,s}$, as probed by transport,[23] optical,[24] scanning tunneling microscopy (STM),[25] inelastic neutron scattering,[26] and angle-resolved photoemission spectroscopy (ARPES) measurements.[14,15] There have been experimental reports showing the persistence of twofold symmetries even above $T_{N,s}$.[15,27–30] In particular, the isovalent-substitution system BaFe$_2$(As$_{1-x}$P$_x$)$_2$ (AsP122)[31] shows an electronic nematic phase transition that breaks the rotational symmetry of the lattice. This transition occurs at a temperature T^*_{Nem} well above $T_{N,s}$ and persists over the superconducting (SC) dome.[27] It should be noted that such a twofold symmetric electronic nematic state has been reported in the PG region of high T_c cuprates.[6]

Although several studies have been reported on the PG formation,[32–40] the PG phase has not been completely established in the phase diagrams of the iron pnictides. In particular,
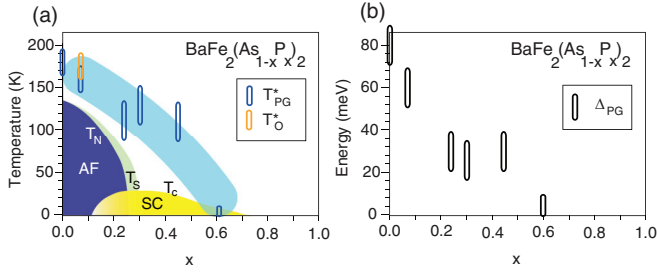
FIG. 1. (Color online) (a) Phase diagram of $BaFe_2(As, P)_2$. Blue and orange markers indicate the temperatures of the PG formation T_{PG}^* and inequivalent energy shift in the zx/yz orbitals T_O^*, respectively. (b) Composition dependence of the PG energy Δ_{PG} obtained by laser ARPES.

only one ARPES study has shown the presence of a normal state energy gap in momentum space for $Ba_{0.75}K_{0.25}Fe_2As_2$ (Ref. [41]). The overall picture of the PG formation in the multiband electronic structure has not been clarified so far. In this paper, we report the PG formation in the momentum-resolved electronic structure of AsP122 and its evolution with temperature and compositions, in pursuit of an as yet unknown PG phase.

Single crystals of $BaFe_2As_2$ (Ba122) were synthesized using the flux method. The starting materials Ba and FeAs were placed in an alumina crucible. This was then sealed in a double quartz tube under 0.3 atmosphere of Ar. The tube was heated at 1273 K for 2 h, slowly cooled to 1073 K for 24 h, and then quenched to room temperature (T).[42] Single crystals of $BaFe_2(As_{1-x}P_x)_2$ with $x = 0.07, 0.24, 0.30, 0.35, 0.45$, and 0.61 were grown by a self-flux method.[31,43] The precursors of Ba_2As_3, Ba_2P_3, FeAs, and FeP were mixed and then sealed in a quartz tube. All the processes were carried out in a glove box filled with dry N_2 gas. The tube was heated at 1150 °C for 10 h and slowly cooled down to 900 °C at a cooling rate 1 °C/h, followed by decanting the flux. The composition of the grown single crystals was confirmed by the energy dispersive x-ray analysis.[43]

Laser ARPES measurements were performed on a spectrometer built using a VG-Scienta R4000WAL electron analyzer and a VUV-laser of 6.994 eV (Ref. [44]) as a photon source at Institute for Solid State Physics (ISSP). Using the $\lambda/2$ (half-wave) plate, we can rotate the light polarization vector and obtain s- or p-polarized light without changing the optical path. The energy resolution was set to $\sim$5 meV to get a high count rate. ARPES measurements at the Brillouin zone (BZ) corner were performed using a spectrometer VG-Scienta R4000WAL electron analyzer, motor-controlled
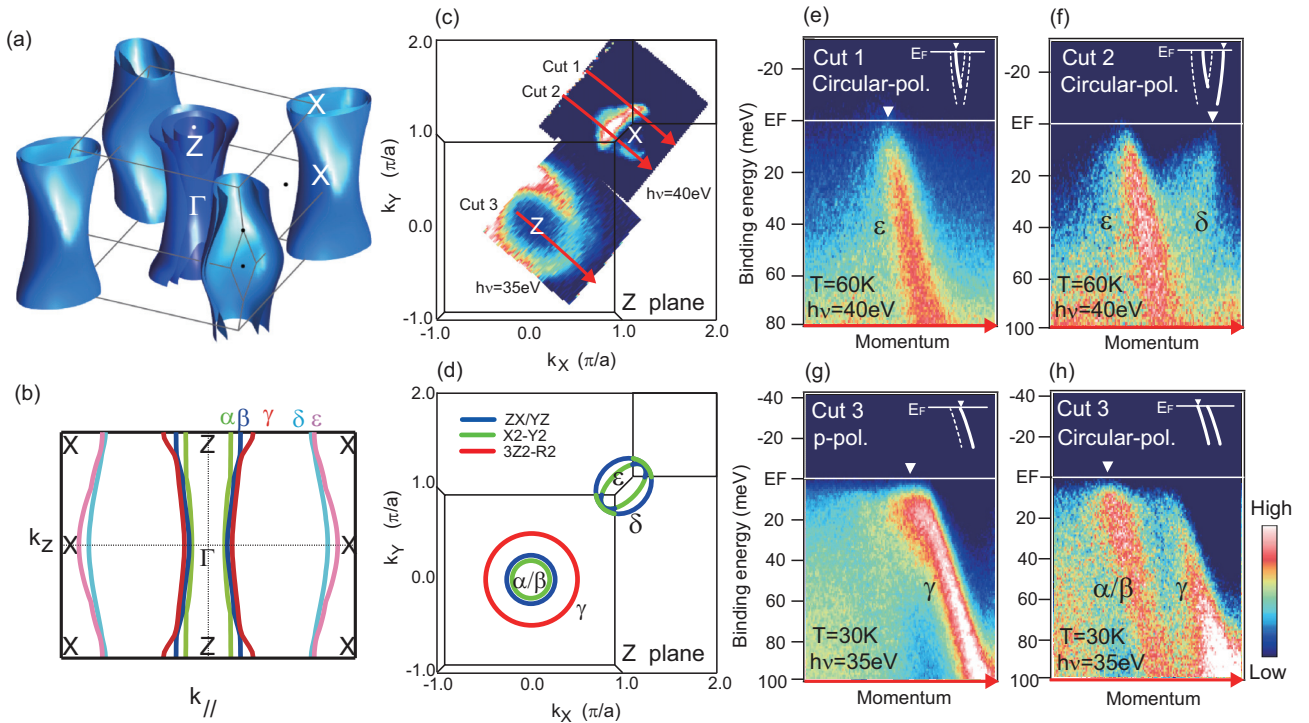

FIG. 2. (Color online) (a) FSs of $BaFe_2(As, P)_2$ for $x = 0.30$ obtained by first principles band calculations. (b) Vertical cut of the calculated FSs. α, β, γ, δ, and ε FSs are colored in green, blue, red, light blue, and purple, respectively. (c) FS mapping in the Z plane taken by p polarization of $h\nu = 35$ eV around the BZ center and circular polarization of $h\nu = 40$ eV around the BZ corner. X, Y in k_X and k_Y represent the tetragonal in-plane momentum axes. (d) Orbital characters on the hole and electron FSs obtained by the first principles band calculations. The schematic FSs are based on ARPES results in (c). Intensity of α and β hole FSs is quite weak in (c) due to the matrix element effect. (e) E-k image along cut 1 in (c) taken by circular polarization at 60 K. (f) E-k image along cut 2 in (c) taken by circular polarization at 60 K. (g) E-k image along cut 3 in (c) taken by p polarization at 30 K. (h) E-k image along cut 3 in (c) taken by circular polarization at 30 K. Insets show the schematic band dispersions illustrating each E-k image. Dotted curves represent the band dispersions whose intensity is suppressed due to the matrix element effect. k_F for each band is indicated by the white triangle. ARPES data were taken at PF BL-28A.

six-axis manipulator and a Helium discharge lamp of $h\nu = 40.8$ eV at University of Tokyo. The energy resolution was set to ~10 meV. The spectra were reproducible over measurement cycles of 12 hours. The Fermi level (E_F) of samples was referenced to that of a gold film evaporated onto the sample holder. The single crystals were cleaved at 200 K in ultrahigh vacuum of ~5×10^{-11} Torr. We did not observe any difference in data even when the crystals were cleaved at the lowest T. Synchrotron-based ARPES measurements were carried out at BL 9A of Hiroshima Synchrotron Radiation Center (HiSOR) and BL 28A of Photon Factory (PF). At HiSOR BL-9A, a VG-Scienta R4000 analyzer and circularly polarized light were used with the total energy resolution of ~8 meV. At PF BL-28A, a VG-Scienta SES-2002 analyzer and circularly and p-polarized light were used with the total energy resolution of ~10 meV. The crystals were cleaved *in situ* at $T \sim 10$ K in an ultrahigh vacuum of ~5×10^{-11} Torr.

The AsP122 system shows quasi-two dimensional FSs above $T_{N,s}$, as shown in Fig. 2(a). Three-hole FSs (α, β, γ) and two-electron FSs (δ, ε) exist around the BZ center and the BZ corner, respectively [Fig. 2(b)]. Substituting As ions by isovalent P ions causes reduction of the pnictogen height without changing the carrier density. As the P concentration is increased, the warping of the γ-hole FS along the k_z axis increases, resulting in a larger FS near the Z plane.[45] Figure 2(c) shows the FS mapping in the Z plane for $x = 0.30$, taken by using the synchrotron radiation photon source (PF BL-28A) of $h\nu = 35$ eV for the BZ center and $h\nu = 40$ eV for the BZ corner. As shown in Fig. 2(d), the hole and electron FSs have different orbital characters depending on the momentum region.

In order to investigate the T dependence of the fine electronic structure in the multiorbital system, it is required to clearly separate the multiple band dispersions. For this purpose, we chose p polarization for the observation of γ band and circular polarization for α/β, δ, and ε bands in the experimental geometries shown in Fig. 2(c). In Figs. 2(e)–2(h), we show the ε, δ, γ, and α/β (nearly degenerate) bands taken along cuts 1–3 in Fig. 2(c), respectively. The Fermi momentum (k_F) was determined at each T by fitting the momentum distribution curves (MDCs) near E_F with a Lorentz function. Note that the energy distribution curves (EDCs) taken at k_F, indicated by the white triangles, can be well separated from the intensity of other bands in the vicinity of E_F.

T dependences of the EDCs at k_F for ε, δ, γ, and α/β bands at $x = 0.30$ are displayed in Figs. 3(a)–3(d). The coherence peak near E_F is clearly observed at low T, especially for the hole bands. If we take a close look at E_F, all of the bands show the depression of the spectral weight with lowering T. In order to extract the intrinsic T-dependent part of the spectral weight, the EDCs are symmetrized with respect to E_F and further normalized by the smoothed EDC recorded at the highest T (150 K), as shown in Figs. 3(e)–3(h). Normalized EDCs in all bands indicate the suppression of the spectral weight near E_F roughly below ~120 K. Since these gaplike structures concomitantly evolve both in the electron and hole bands, the T-dependent gapped feature in the EDCs in the normal state should be then attributed to PG formation in the total density of states. We thus consider that the hole and electron bands show nearly comparable PGs of ~20 meV for optimally doped AsP122.
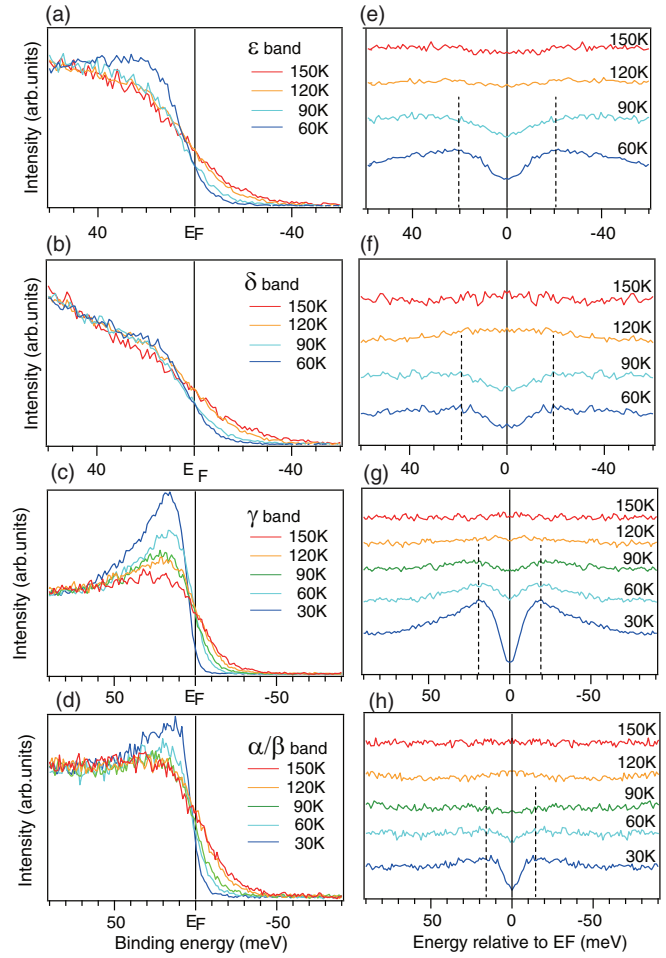

FIG. 3. (Color online) (a–d) T dependence of the EDCs for $x = 0.30$ measured at k_F of the ε band in Fig. 2(e), δ band in Fig. 2(f), γ band in Fig. 2(g), and the α/β band in Fig. 2(h), respectively. (e–h) The EDCs in (a–d) symmetrized with respect to E_F and further normalized by the smoothed EDC at 150 K, respectively. Broken lines indicate the PG energy. Note the larger x-axis energy scale for γ and α/β bands [panels (c, g) and (d, h)]. ARPES data were taken at PF BL-28A.

In order to investigate how the PG evolves in the phase diagram, here we use laser ARPES (ISSP) of $h\nu = 6.994$ eV and detect the electronic structure of the γ-hole band near the Z plane ($3Z^2$-R^2 orbital) for $x = 0.00$–0.61 [Fig. 4(a)].[46,47] By choosing the s-polarized laser as the photon source, we can successfully separate the γ-hole band from other bands [Figs. 4(b)–4(d)], owing to the distinct orbital characters of the hole FS sheets[48] and selection rules for ARPES.[49] Here we focus on the γ-hole band for investigating its T dependence at $x = 0.00$ ($T_{N,s} = 136$ K), 0.07 ($T_{N,s} = 114$ K), 0.24 ($T_{N,s} = 55$ K, $T_c = 16$ K), 0.30 ($T_c = 30$ K), 0.45 ($T_c = 22$ K), and 0.61 ($T_c = 9$ K) of AsP122.

Figures 5(a)–5(c) show the T dependence of the EDCs at k_F in the γ-hole band at $x = 0.07$, 0.30, and 0.61. EDCs at $x = 0.61$ clearly intersect at E_F, as simply expected by the T dependence of the Fermi-Dirac (FD) distribution [Fig. 5(c)]. In contrast, EDCs at $x = 0.07$ in Fig. 5(a) exhibit drastic T dependence below ~150 K. As shown in the inset, the spectral weight at E_F decreases with lowering T, indicating
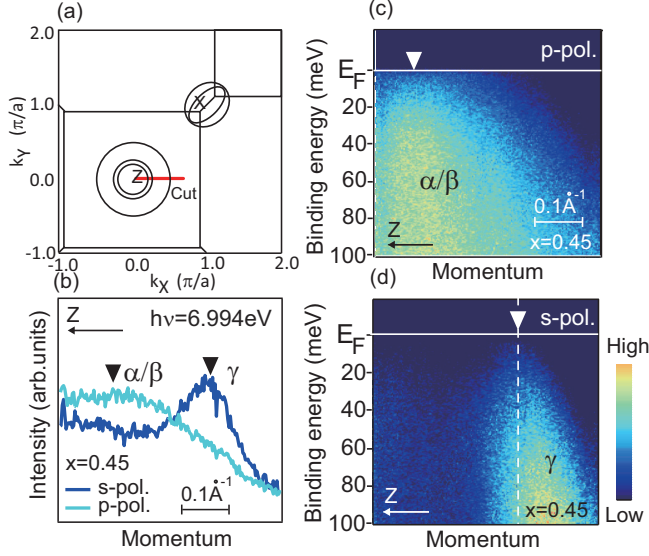
FIG. 4. (Color online) (a) Schematics of the in-plane cut of FS sheets in the Z plane of BaFe$_2$(As, P)$_2$. Red line indicates the momentum region measured by laser ARPES (ISSP) for $0.07 \leq x \leq 0.61$. Only for $x = 0.00$, the measured momentum cut is rotated by 45°. (b) MDCs at E_F for $x = 0.45$ recorded by s (blue) and p (light blue) polarizations along momentum cut shown in (a). Black triangles indicates k_F for α/β- and γ-hole bands, determined by the peak positions of the MDCs. α- and β-hole bands are nearly degenerate. (c), (d) Hole bands at $x = 0.45$ measured along the momentum cut shown in (a) by using p and s polarizations, respectively. The γ-hole band can be separately observed by choosing s polarization in the experimental geometry shown in (a). The EDCs in the γ-hole band were obtained at k_F, as indicated by broken white line in (d).

FIG. 5. (Color online) (a–c) T dependence of the EDCs at k_F of the γ-hole band measured by laser ARPES (ISSP) for $x = 0.07$, 0.30, and 0.61, respectively. Inset shows the spectra near E_F in an enlarged energy scale. (d–f) EDCs symmetrized with respect to E_F and further normalized by the smoothed EDC at the highest T. Black arrow indicates the crossing point of the spectra with decreasing T, representing the PG energy. Note the larger x-axis energy scale for $x = 0.07$ [panels (a) and (d)].

the evolution of a gaplike structure. Similar T dependences are also observed for $x = 0.30$ [Fig. 5(b)], although the gaplike structure itself becomes weaker with increasing x. This result indicates that the gaplike structure exists in a wide T and x region, which seems to disappear toward $x \sim 0.6$.

The EDCs are symmetrized with respect to E_F and further normalized by the smoothed EDC recorded at the highest T (200, 170, 180 K for $x = 0.07$, 0.30, and 0.61), as shown in Figs. 5(d)–5(f). The symmetrized EDCs for $x = 0.61$ again indicate T-independent spectral weight similar to normal metal, thus showing the accuracy and the validity of the data analysis. The symmetrized EDCs at 0.07 and 0.30 clearly show the depression of the spectral weight in the normal state, consistent with the PG formation in the synchrotron-based ARPES (Fig. 3). However, the coherence peak of the γ-hole band is not apparent in the case of laser ARPES, which may be possibly due to the matrix element effect.

The PG appears around a certain temperature T_{PG}^*. For example, at $x = 0.07$, the symmetrized EDC at $T = 150$ K slightly shows a gap feature near E_F, while those at $T = 170$ K and 200 K remain unchanged. T_{PG}^* is thus estimated to be between 150 K and 170 K. Here we quantitatively estimate T_{PG}^* for each P concentration. Figures 6(a)–6(f) show the symmetrized EDCs [same as the spectra in Figs. 5(d)–5(f)] with offsets and zero lines (horizontal black line) superimposed on respective curves as references to focus on the T-dependent part of the spectra. The black area in each
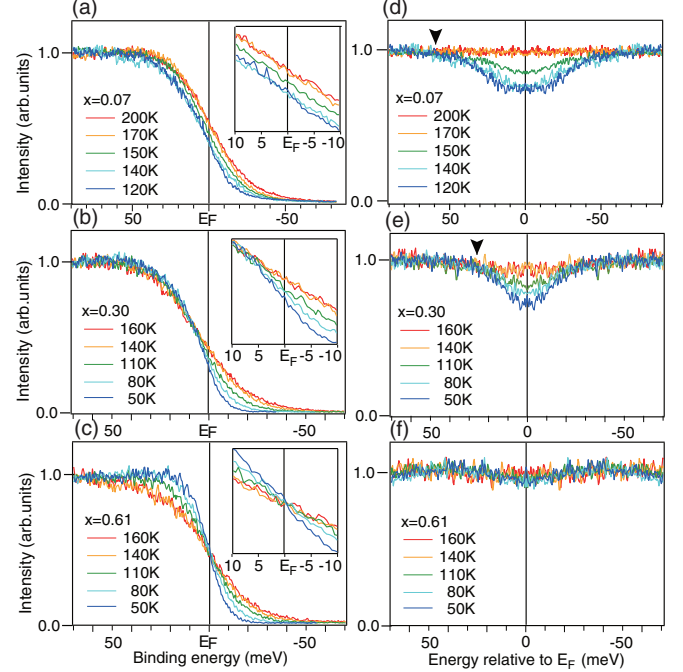
spectrum indicates the decrease of the spectral weight with lowering T, which should represent the PG formation. Here we note that previous ARPES studies reported an anomalous band shift with increasing T toward room temperature on Ru-doped Ba122 (Ref. 50) and Co-doped Ba122 systems.[51] In this paper, we are discussing the T-dependent spectral weight near E_F separately from such band shift effect by closely tracking the T-dependent band dispersion crossing E_F. We also note that the temperature ranges of the PG formation ($T_{PG}^* \leq 180$ K) and the band shift (up to 300 K) are not identical. This fact seems to indicate that these two phenomena are different in origin, which should be further investigated for understanding the anomalous T-dependent electronic structures. Now we evaluate the T and x dependence of the PG. It is clear that the PG persists up to $T_{PG}^* \sim 180$ K for $x = 0.00$ ($T_{N,s} = 136$ K), ~ 160 K for 0.07 ($T_{N,s} = 114$ K), and ~ 110 K for 0.24 ($T_{N,s} = 55$ K), as indicated by the spectra in the light blue area of Figs. 6(a)–6(c). This is indicative of a PG phase extending much above $T_{N,s}$. The PG is still observed for further doped $x = 0.3$ and 0.45, where the magnetostructural transition no longer exists but eventually disappears at $x = 0.61$, at least above 10 K. In Figs. 6(g)–6(l), we plot the T dependence of the gapped area S as a measure of PG formation, which is estimated by integrating the black area in Figs. 6(a)–6(f). T_{PG}^* estimated from the onset T of the PG formation are plotted onto the phase diagram in Fig. 1(a). The obtained phase diagram of AsP122 clearly shows a PG phase extending above $T_{N,s}$ and T_c in a wide range of $0.00 \leq x < 0.61$.
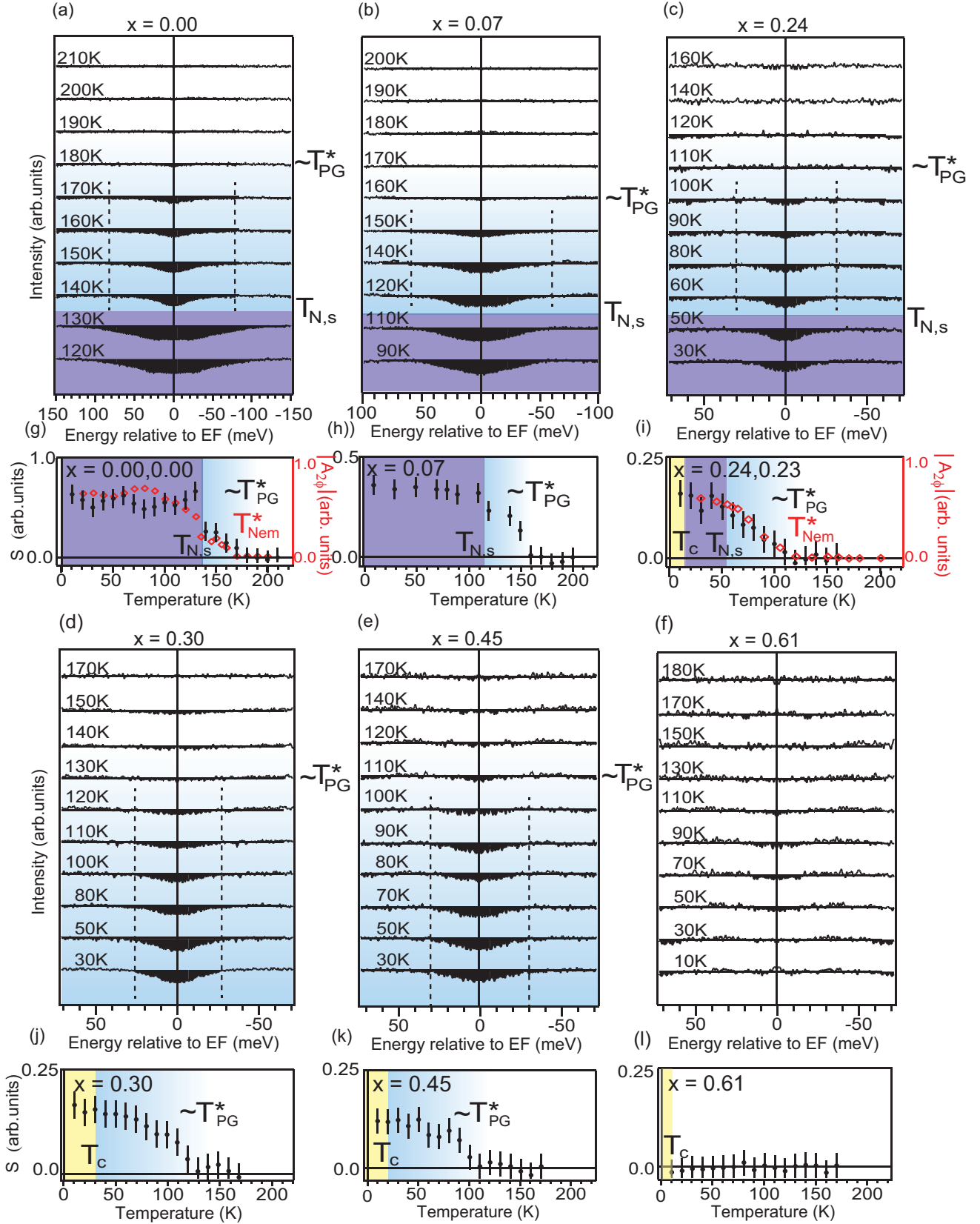
FIG. 6. (Color online) (a–f) Symmetrized and normalized EDCs measured by laser ARPES (ISSP) for $x = 0.00, 0.07, 0.24, 0.30, 0.45$, and 0.61, respectively. The T-dependent depression of the spectral weight is indicated by the black shaded area. Note the larger x-axis energy scale for $x = 0.0$ and 0.07 [panels (a) and (b)]. Dotted lines indicate PG energy. (g–l) T dependence of S, the gapped area. T^*_{PG} is defined by the temperature at which S starts to evolve. Twofold oscillation amplitudes of the torque for $x = 0.00$ and 0.23 (Ref. 27) are superimposed in (g) and (i), respectively. The background of each panel is colored in light blue for $T_{N,s} < T < T^*_{PG}$, blue for $T_c < T < T_{N,s}$, and yellow for $T < T_c$.
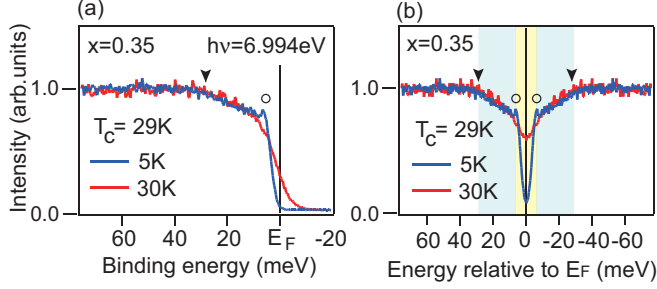
FIG. 7. (Color online) (a) The EDCs of the γ-hole band measured at 5 K ($T < T_c$) and 30 K ($T_c < T$) for $x = 0.35$ by laser ARPES (ISSP). The black arrow and open circle represent the energy position of the PG and SC gap, respectively. (b) The EDCs symmetrized with respect to E_F. Light blue and yellow areas highlight the energy scale of the PG and SC gap, respectively.

Recent torque magnetometry and x-ray diffraction measurements reported that twofold symmetric properties in the lattice and magnetic response appear at $T_{\text{Nem}}^* (> T_{N,s})$ (Ref. 27). Twofold oscillation amplitudes of the torque for $x = 0.00$ and 0.23 are superimposed on Figs. 6(g) and 6(i), respectively. The good correspondence between T_{Nem}^* and T_{PG}^* in Figs. 6(g) and 6(i) reveals that such electronic nematic phase can be closely related to the PG observed by laser ARPES, especially in the underdoped region.

The energy scale of the PG, Δ_{PG}, can be also estimated from the crossing point of the symmetrized EDCs, as indicated by the black arrows in Figs. 5(d) and 5(e). As summarized in Fig. 1(b), this indicates that the PG tends to decrease from $\Delta_{\text{PG}} \sim 60$ meV to $\Delta_{\text{PG}} \sim 25$ meV, with increasing P concentration from $x = 0.07$ to $x = 0.30$. Here we discuss the energy scales of the PG and SC gaps in the AsP122 system. EDCs in the γ-hole band below and above T_c for $x = 0.35$ are shown in Fig. 7(a). Both EDCs show a broad hump structure around ~ 30 meV (black arrow), indicative of the PG formation. In addition, the SC gap appears around ~ 5 meV with a small coherent peak (open circle) in the EDC below T_c. Symmetrization of the EDCs in Fig. 7(b) clearly demonstrates that the PG energy is much larger than SC gap magnitude in AsP122.

Synchrotron-based $h\nu$-dependent ARPES reveals that the PG structure in the EDCs are similarly found in the α/β hole FS around the BZ center. k_F positions measured by photons of $h\nu = 16$–38 eV (HiSOR BL-9A and PF BL-28A) are superimposed on the calculated FSs in Fig. 8(a). Symmetrized EDCs shown in Fig. 8(b) were taken at k_F of different k_z values in α/β hole FS for $x = 0.30$ below T_c. The hump structures ranging from 18 meV to 30 meV (black arrows) are signatures of the PG formation. In particular, the shoulder structure around 5–8 meV (open circles) indicates an SC gap opening, consistent with previous ARPES measurements.[46,47,52] Synchrotron-based ARPES thus shows that the SC gap in AsP122 is smaller than the PG, consistent with laser ARPES. A PG with an energy scale higher than the SC gap has been also reported for a variety of iron-based superconductors by several experimental probes.[32,33,35,36,39,40]

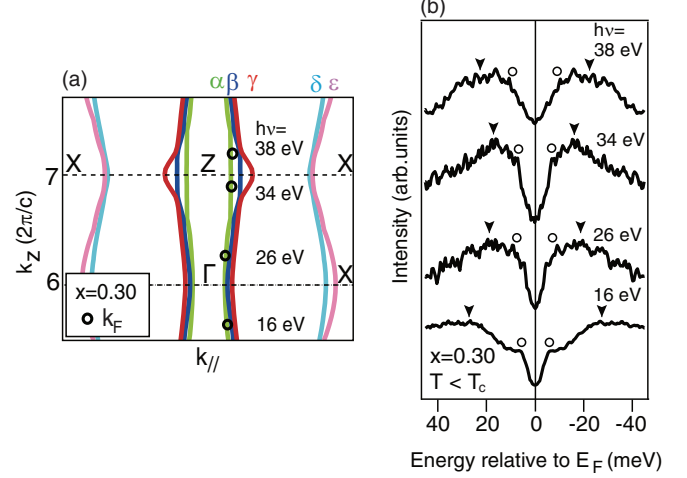The difference in the energy scales of the PG and SC gaps in several FSs implies that the PG formation is not simply

FIG. 8. (Color online) (a) Schematics of the FSs obtained by the first principles band calculations for $x = 0.30$. k_F positions in the α/β hole FSs at which the data in (b) were obtained are plotted by the open circles. (b) Symmetrized EDCs taken at k_F in the α/β hole FSs for $x = 0.30$ below T_c by using photons of $h\nu = 16$ eV, 26 eV (HiSOR BL-9A) and 34 eV, 38 eV (PF BL-28A). Black arrows and open circles represent the energy scale of the PG and SC gap, respectively.

a precursor of the SC electron pairing.[4–6] According to T_{PG}^* and Δ_{PG} values in Figs. 1(a) and 1(b), we can estimate the $2\Delta_{\text{PG}}/k_B T_{\text{PG}}^*$ as ~ 10.3 for $x = 0.00$, ~ 8.7 for $x = 0.07$, ~ 6.7 for $x = 0.24$, ~ 4.5 for $x = 0.30$, and ~ 6.3 for $x = 0.45$. Relatively high values for $x = 0.00$ and 0.07 imply the importance of magnetism for the PG formation. Indeed, the T dependence of $1/T_1 T$ in nuclear magnetic resonance measurements suggests that the AF fluctuations are enhanced above T_N in the underdoped region.[53,54]

One may consider that the energy scale of the PG reflects that of the AF gap below T_N. Previous ARPES[14,55] and dHvA[56] measurements on Ba122 reported highly three-dimensional disconnected FSs in the AF state. Across the magnetostructural transition, most of the bands of Ba122 are drastically pushed away from E_F, in contrast to other bands still remaining near E_F, as predicted by the first principles band calculations.[14] According to our T-dependent laserARPES on Ba122, the hole band in which we observed the PG in this paper intersects E_F even in the AF state (not shown). It forms a part of the three-dimensional FSs, and spectral intensity at E_F is still finite, which is far from a fully opened gap feature. On the other hand, the band calculations[14,57] also show several gap structures around ~ 100 meV in the density of states in the AF state. Such gap formations are consistent with the optical conductivity data,[24,58] which were interpreted as the various optical transitions between the reconstructed Fe 3d bands. The magnitude of the gaps in the density of states in the AF state is comparable to that of the PG.

It is also worth mentioning that the energy scale of the PG is comparable to that of the anisotropic energy shift of the zx and yz orbitals observed at the BZ corner. Such orbital inequivalency in the zx/yz orbitals induces a rotational symmetry breaking, which is one of the possible origins of the electronic nematicity. The lifting of the yz and zx orbital degeneracy in the band structure at the tetragonal BZ
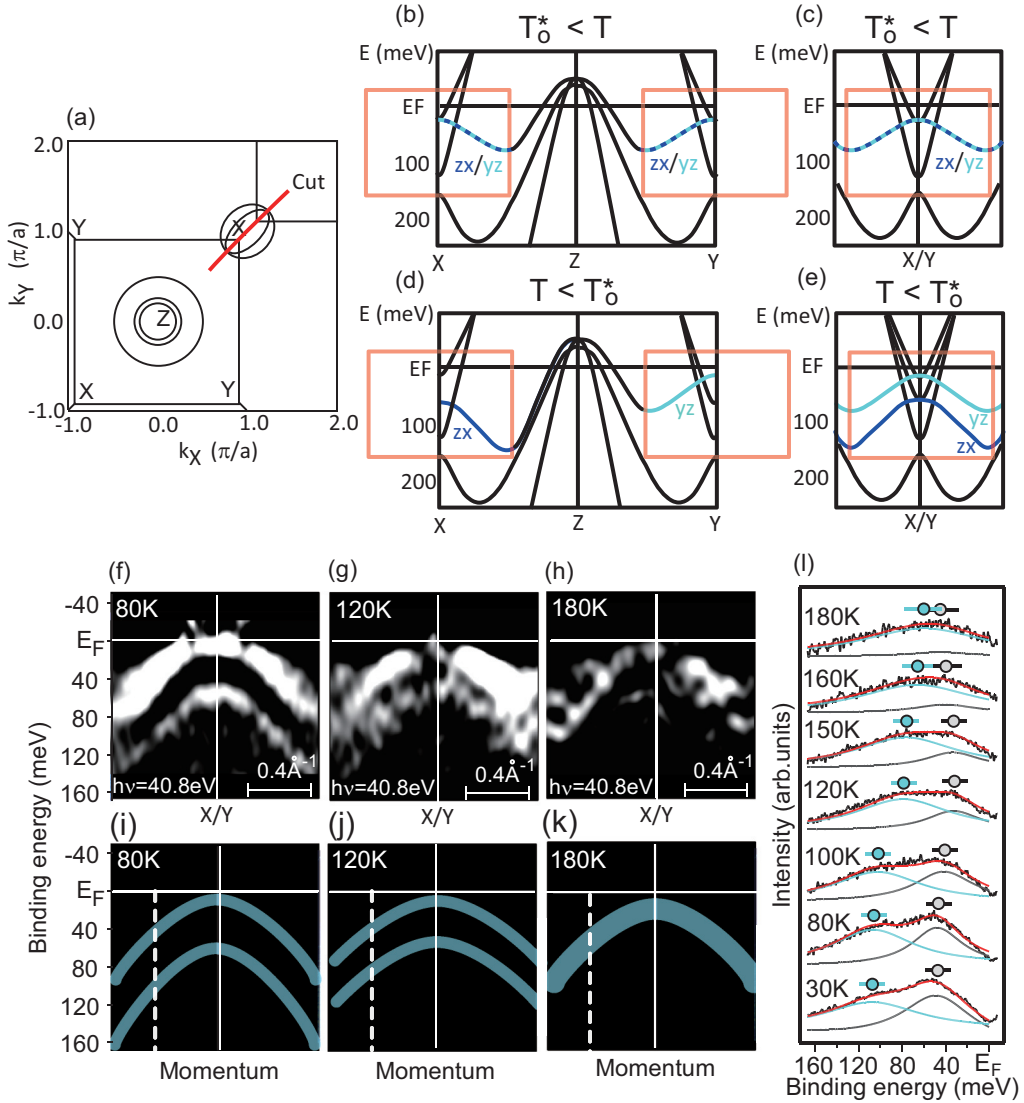
FIG. 9. (Color online) (a) Schematics of the in-plane cut of FS sheets in the Z plane of $BaFe_2(As, P)_2$. The red line indicates the momentum region measured by helium-lamp ARPES for $x = 0.07$. (b), (c) Schematic band dispersions above T_O^* for detwinned and twinned crystals, respectively, where T_O^* represents the temperature at which the zx/yz bands start to show an inequivalent energy shift. Red rectangles represent the E-k region of the ARPES data shown in (f-h). (d), (e) Schematic band dispersions with orbital-dependent energy shift at BZ corners below T_O^* for detwinned and twinned crystals, respectively. This picture was originally shown in Ref. 15 for Ba122 parent material. Energy positions of the zx and yz bands in (b–e) are modified, taking into account our ARPES results on P-substituted Ba122 system. (f) Band dispersion (second derivative) at the BZ corner near the Z plane measured by Helium discharge lamp ARPES (University of Tokyo) of $h\nu = 40.8$ eV at 80 K ($T < T_{N,s}$). (g) The same measured at 120 K ($T_{N,s} < T < T_{PG}^*$). (h) The same measured at 180 K ($T_{PG}^* < T$). (i–k) Schematics of the band dispersions corresponding to (f–h), respectively. Two hole bands (light blue curves) are observed at low T. Note that intensity of δ and ε electron bands crossing E_F is weak in this experimental geometry. (l) T dependence of the EDCs divided by FD function at the momentum cut indicated by the broken white line in (i–k). Linear back ground was subtracted from each spectrum. Red curves represent the fitting functions composed of double Lorentz functions illustrated by gray and light blue curves. Gray and light blue circles represent the peak positions in the EDCs obtained by the fitting procedure, indicating the energy position of upper and lower hole band, respectively.

corner had been discussed in a previous ARPES study on $Ba(Fe,Co)_2As_2$ (FeCo122) (Ref. 15). Owing to the detwinning technique and polarization-dependent measurements, they separately observed the two bands below E_F at $(\pi, -\pi)$ point (Y point) and (π, π) point (X point), indicating the zx and yz character, respectively.[15] Such an inequivalent shift in the energy of the zx/yz orbitals were observed even above $T_{N,s}$, implying the development of the zx/yz orbital order from high T. Recent x-ray absorption measurements on FeCo122

system also reported differences in the occupation of the zx/yz orbitals above $T_{N,s}$ (Ref. 30).

Here we directly confirm the orbital inequivalency in AsP122 in relation to the existence of the PG phase. Since the detwinning by uniaxial pressure is known to raise the onset T of the anisotropy,[15,59] here we chose twinned crystals to precisely compare with the phase diagram of the PG. A previous ARPES study confirmed that AsP122 has two electron bands (δ, ε) forming FSs around the BZ corner.[45] Along the

momentum cut in Fig. 9(a), photoelectoron intensities of those electron bands are relatively weak due to the matrix element effect. We thus chose this experimental geometry in order to emphasize the zx/yz hole bands just below E_F around the BZ corner.

Here we briefly describe how the orbital anisotropy can be observed in the twinned samples by referring to the reported case of Ba122 parent material.[15] The energy positions of the zx and yz bands at the BZ corner in schematics shown in Figs. 9(b)–9(e) roughly correspond to our ARPES results on P-substituted Ba122 system. Figures 9(b) and 9(c) show the schematic band dispersions in the tetragonal phase for detwinned and twinned crystals, respectively. Here, the zx and yz orbitals are degenerate, reflecting a tetragonal symmetry. Therefore, there is naturally no difference in the E-k image between detwinned and twinned crystals. On the other hand, Figs. 9(d) and 9(e) show schematic band dispersions with orbital-dependent energy shift below T_O^* for detwinned and twinned crystals, respectively. T_O^* represents the temperature at which the zx/yz bands start to show the inequivalent energy shift. Below T_O^*, the zx orbital around the X point and the yz orbital around the Y point show different energy shifts [Fig. 9(d)], as reported in the case for Ba122 (Ref. [15]). In the case of twinned crystals, the X and Y points are overlapped in the momentum space, thus resulting in both the zx and yz bands with different energy levels appearing in one momentum cut across the BZ corner [Fig. 9(e)]. Then, the difference in energy between these two hole bands represents the anisotropic electronic occupation in the zx/yz orbitals.

Shown in Figs. 9(f)–9(h) are the band dispersions (second derivative) at the tetragonal BZ corner near the Z plane taken along the momentum cut indicated in Fig. 9(a) for $x = 0.07$ measured at 80 K, 120 K, and 180 K, respectively. Corresponding E-k region is represented by the red rectangles in Figs. 9(b)–9(e). Two hole bands are clearly observed below E_F in the ARPES image at 80 K ($T < T_{N,s}$) in Fig. 9(f) [see also Fig. 9(i)]. Note that both the zx/yz hole bands below E_F at X and Y point appear in the same image, as described in Fig. 9(e). Importantly, the hole bands remain well separated even at 120 K ($T_{N,s} < T < T_{PG}^*$) [Figs. 9(g) and 9(j)]. At 180 K ($T_{PG}^* < T$), such a clear separation is not observed, indicating that the two bands are degenerate within experimental accuracy [see Figs. 9(h) and 9(k)].

Focusing on the energy positions of the two hole bands, we investigated the T dependence of the EDCs at a certain momentum indicated by the broken white lines in Figs. 9(i)–9(k). We plotted the EDC peak positions from 30 K to 180 K by fitting them using double Lorentz functions, as shown in Fig. 9(l). EDCs were divided by FD functions, and a linear background was subtracted from each spectrum. Two peaks are marked by black (upper hole-band) and light blue (lower hole-band) circles. The difference in energy between upper and lower hole bands decreases as T increases, as summarized in Fig. 10. While two hole bands are well separated at low T, they become nearly degenerate around 160–180 K. The observation of the nearly degenerate bands splitting into two hole bands at the BZ corner on cooling thus corresponds to the T-dependent inequivalent energy shift in the zx/yz orbitals possibly related to orbital ordering, as was predicted theoretically.[20–22] We find that the inequivalent energy shift
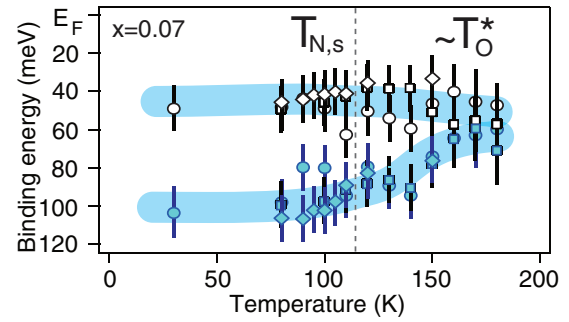

FIG. 10. (Color online) T dependence of the energy position of the two hole bands below E_F around the BZ corner. Gray and light blue symbols represent the peak positions in the EDCs along a white broken line in Fig. 9 (i–k) for upper and lower hole-bands, respectively. Circles, diamonds, and squares represent the data obtained from different samples. T_O^* is estimated to be 160 K ~ 180 K.

in the zx/yz orbitals is similar in magnitude to the PG in the $3Z^2$-R^2 orbital. It also sets in around $T_O^* \sim$ 160 K–180 K, nearly comparable to T_{PG}^*. Although T_O^* and T_{PG}^* show large error bars due to the crossoverlike behavior, these temperatures are close to T_{Nem}^* (Ref. [27]). This result implies that the rotational symmetry breaking in AsP122 occurs not only in the lattice and magnetism, but also in the orbital, and may be related to the PG formation.

In this paper, we confirmed the PG formation in the momentum-resolved multiband electronic structure of optimally doped AsP122. Hole FSs around the BZ center and electron FSs near the BZ corner in the Z plane commonly exhibit PG formation with a comparable energy scale of ~20 meV. The energy scale of the PG is larger than that of SC gap, suggesting that it is not a precursor of the SC pairing. The present results in which the PG exists in all bands in the Z plane (Fig. 3) and at any k_z position in the hole bands (Fig. 8) suggest that the PG should appear in the total density of states as well.

We further found the PG phase well above $T_{N,s}$ and T_c. The shape of the PG phase diagram looks like that of the AF phase extended in a wider T and x region, especially in the underdoped region, as is the case for the cuprates. It implies that the AF fluctuation should be a key ingredient for PG formation. In cuprates, ARPES measurements reported the PG formation temperature above the SC dome.[60] Then it has been suggested that the appearance of the electronic nematicity is associated with the PG formation by neutron scattering,[61] STM,[62] and Nernst effect[6] measurements. Therefore our results indicate that the PG phase and the electronic nematicity appear to be common features of high T_c superconductivity, both in cuprates and iron pnictides.

However, there is a crucial difference between the two systems. In AsP122, the inequivalent energy shift in the zx/yz orbitals is observed below $T_O^* \sim T_{PG}^*$ [and also $\sim T_{Nem}^*$ (Ref. [27])] for $x = 0.07$ [Fig. 1(a)]. This implies that the origin of the PG is likely to be linked to the orbital ordering, which may give rise to the in-plane anisotropic spin and/or orbital fluctuations causing the PG formation. A similar situation has also been theoretically discussed for the nematic

phase.[63,64] Complex coupling of spin, orbital, and lattice[22,65] for respective compounds should be taken into account for further quantitative comparison. We stress that such orbital-related mechanism is not applicable to cuprates composed of a single $d_{x^2-y^2}$ orbital.

It is notable that the PG phase in AsP122 is robust over the SC phase. On the contrary, the PG of $BaKFe_2As_2$ (BaK122), which was reported for underdoped $x = 0.25$ (Ref. [41]), has not been found in optimal doping so far. Although the PG phase in BaK122 is still not completely established, it may indicate that the PG phase of BaK122 is much more suppressed than AsP122.

Possible variety of the PG phase in Ba122 family can be consistently classified in relation to the electronic nematic phase. Actually, nearly isotropic in-plane electronic resistivity is reported in underdoped BaK122 (Refs. [66–68]), indicative of a small contribution of the electronic nematicity. At least in the Ba122 family, a close relationship between PG formation and electronic nematicity is expected, although it seems to strongly depend on the character of the substitution ions. Understanding how the PG formation and orbital inequivalency reported here influence the normal state physical properties, which in turn should affect the variety of the SC gap symmetry in iron-based superconductors, is therefore a pressing issue that deserves comprehensive studies of high T_c superconductivity.

---

*Corresponding author: shimojima@ap.t.u-tokyo.ac.jp

[1] T. Timusk and B. Statt, Rep. Prog. Phys. **62**, 61 (1999).

[2] M. R. Norman, D. Pines, and C. Kallin. Adv. Phys. **54**, 715 (2005).

[3] S. Hüfner, M. A. Hossain, A. Damascelli, and G. A. Sawatzky, Rep. Prog. Phys. **71**, 062501 (2008).

[4] M. Randeria, *Proceedings of the International School of Physics, Enrico Fermi Course CXXXVI on High Temperature Superconductors*, edited by G. Iadonisi, J. R. Schrieffer, and M. L. Chiafalo, (IOS Press, Amsterdam, 1999), p. 53.

[5] V. J. Emery and S. A. Kivelson, Nature **374**, 434 (1995).

[6] R. Daou, J. Chang, D. LeBoeuf, O. Cyr-Choinière, F. Lalibertè, N. Doiron-Leyraud, B. J. Ramshaw, R. Liang, D. A. Bonn, W. N. Hardy, and L. Taillefer, Nature **463**, 519 (2010).

[7] J. E. Hoffman, E. W. Hudson, K. M. Lang, V. Madhavan, H. Eisaki, S. Uchida, and J. C. Davis, Science **295**, 466 (2002).

[8] M. Vershinin, S. Misra, S. Ono, Y. Abe, Y. Ando, and A. Yazdani, Science **303**, 1995 (2004).

[9] C. Howald, H. Eisaki, N. Kaneko, M. Greven, and A. Kapitulnik, Phys. Rev. B **67**, 014533 (2003).

[10] J. G. Bednorz and K. A. Muller, Z. Phys. B **64**, 189 (1986).

[11] Y. Kamihara, T. Watanabe, M. Hirano, and H. Hosono, J. Am. Chem. Soc. **130**, 3296 (2008).

[12] C. de la Cruz, Q. Huang, J. W. Lynn, J. Li, W. Ratcliff, II, J. L. Zarestky, H. A. Mook, G. F. Chen, J. L. Luo, N. L. Wang, and P. Dai, Nature **453**, 899 (2008).

[13] D. J. Singh and M.-H. Du, Phys. Rev. Lett. **100**, 237003 (2008).

[14] T. Shimojima, K. Ishizaka, Y. Ishida, N. Katayama, K. Ohgushi, T. Kiss, M. Okawa, T. Togashi, X.-Y. Wang, C.-T. Chen, S. Watanabe, R. Kadota, T. Oguchi, A. Chainani, and S. Shin, Phys. Rev. Lett. **104**, 057002 (2010).

[15] M. Yi, D. Lu, J.-H. Chu, J. G. Analytis, A. P. Sorini, A. F. Kemper, B. Moritz, S.-K. Mo, R. G. Moore, M. Hashimoto, W.-S. Lee, Z. Hussain, T. P. Devereaux, I. R. Fisher, and Z.-X. Shen, PNAS **108**, 6878 (2011).

[16] I. I. Mazin, D. J. Singh, M. D. Johannes, and M. H. Du, Phys. Rev. Lett. **101**, 057003 (2008).

[17] K. Kuroki, S. Onari, R. Arita, H. Usui, Y. Tanaka, H. Kontani, and H. Aoki, Phys. Rev. Lett. **101**, 087004 (2008).

[18] H. Kontani and S. Onari, Phys. Rev. Lett. **104**, 157001 (2010).

[19] Y. Yanagi, Y. Yamakawa, and Y. Ōno, Phys. Rev. B **81**, 054518 (2010).

[20] F. Kruger, S. Kumar, J. Zaanen, and J. vandenBrink, Phys. Rev. B **79**, 054504 (2009).

[21] W. Lv, J. Wu, and P. Phillips, Phys. Rev. B **80**, 224506 (2009).

[22] C.-C. Lee, W.-G. Yin, and W. Ku, Phys. Rev. Lett. **103**, 267001 (2009).

[23] J.-H. Chu, J. G. Analytis, K. D. Greve, P. L. McMahon, Z. Islam, Y. Yamamoto, and I. R. Fisher, Science **329**, 824 (2010).

[24] M. Nakajima, T. Liang, S. Ishida, Y. Tomioka, K. Kihou, C. H. Lee, A. Iyo, H. Eisaki, T. Kakeshita, T. Ito, and S. Uchida, PNAS **108**, 12238 (2011).

[25] T.-M. Chuang, M. P. Allan, J. Lee, Y. Xie, N. Ni, S. L. Bud'ko, G. S. Boebinger, P. C. Canfield, and J. C. Davis, Science **327**, 181 (2010).

[26] J. Zhao, D. T. Adroja, D.-X. Yao, R. Bewley, S. Li, X. F. Wang, G. Wu, X. H. Chen, J. Hu, and P. Dai, Nature Physics **5**, 555 (2009).

[27] S. Kasahara, H. J. Shi, K. Hashimoto, S. Tonegawa, Y. Mizukami, T. Shibauchi, K. Sugimoto, T. Fukuda, T. Terashima, A. H. Nevidomskyy, and Y. Matsuda, Nature **486**, 382 (2012).

[28] M. Yi, D. H. Lu, R. G. Moore, K. Kihou, C.-H. Lee, A. Iyo, H. Eisaki, T. Yoshida, A. Fujimori, and Z.-X. Shen, New J. Phys. **14**, 073019 (2012).

[29] Y. Zhang, C. He, Z. R. Ye, J. Jiang, F. Chen, M. Xu, Q. Q. Ge, B. P. Xie, J. Wei, M. Aeschlimann, X. Y. Cui, M. Shi, J. P. Hu, and D. L. Feng, Phys. Rev. B **85**, 085121 (2012).

[30] Y. K. Kim, W. S. Jung, G. R. Han, K.-Y. Choi, K.-H. Kim, C.-C. Chen, T. P. Devereaux, A. Chainani, J. Miyawaki, Y. Takata,

Y. Tanaka, M. Oura, S. Shin, A. P. Singh, H. G. Lee, J.-Y. Kim, and C. Kim, Phys. Rev. Lett. **111**, 217001 (2013).

[31] S. Kasahara, T. Shibauchi, K. Hashimoto, K. Ikada, S. Tonegawa, R. Okazaki, H. Shishido, H. Ikeda, H. Takeya, K. Hirata, T. Terashima, and Y. Matsuda, Phys. Rev. B **81**, 184519 (2010).

[32] Y. Ishida, T. Shimojima, K. Ishizaka, T. Kiss, M. Okawa, T. Togashi, S. Watanabe, X. Wang, C. Chen, Y. Kamihara, M. Hirano, H. Hosono, and S. Shin, J. Phys. Soc. Jpn. **77**, Suppl. C 61 (2008).

[33] T. Sato, K. Nakayama, Y. Sekiba, T. Arakane, K. Terashima, S. Souma, T. Takahashi, Y. Kamihara, M. Hirano, and H. Hosono, J. Phys. Soc. Jpn. **77**, Suppl. C 65 (2008).

[34] K. Ahilan, F. L. Ning, T. Imai, A. S. Sefat, R. Jin, M. A. McGuire, B. C. Sales, and D. Mandrus, Phys. Rev. B **78**, 100501(R) (2008).

[35] D. R. Garcia, C. Jozwiak, C. G. Hwang, A. Fedorov, S. M. Hanrahan, S. D. Wilson, C. R. Rotundu, B. K. Freelon, R. J. Birgeneau, E. Bourret-Courchesne, and A. Lanzara, Phys. Rev. B **78**, 245119 (2008).

[36] T. Mertelj, V. V. Kabanov, C. Gadermaier, N. D. Zhigadlo, S. Katrych, J. Karpinski, and D. Mihailovic, Phys. Rev. Lett. **102**, 117002 (2009).

[37] M. A. Tanatar, N. Ni, A. Thaler, S. L. Bud'ko, P. C. Canfield, and R. Prozorov, Phys. Rev. B **82**, 134528 (2010).

[38] S.-H. Baek, H.-J. Grafe, L. Harnagea, S. Singh, S. Wurmehl, and B. Büchner, Phys. Rev. B **84**, 094510 (2011).

[39] Y.-C. Wen, K.-J. Wang, H.-H. Chang, J.-Y. Luo, C.-C. Shen, H.-L. Liu, C.-K. Sun, M.-J. Wang, and M.-K. Wu, Phys. Rev. Lett. **108**, 267002 (2012).

[40] S. J. Moon, A. A. Schafgans, S. Kasahara, T. Shibauchi, T. Terashima, Y. Matsuda, M. A. Tanatar, R. Prozorov, A. Thaler, P. C. Canfield, A. S. Sefat, D. Mandrus, and D. N. Basov, Phys. Rev. Lett. **109**, 027006 (2012).

[41] Y.-M. Xu, P. Richard, K. Nakayama, T. Kawahara, Y. Sekiba, T. Qian, M. Neupane, S. Souma, T. Sato, T. Takahashi, H.-Q. Luo, H.-H. Wen, G.-F. Chen, N.-L. Wang, Z. Wang, Z. Fang, X. Dai, and H. Ding, Nat. Commun. **2**, 392 (2011).

[42] K. Ohgushi and Y. Kiuchi, Phys. Rev. B **85**, 064522 (2012).

[43] M. Nakajima, S. Uchida, K. Kihou, C.-H. Lee, A. Iyo, and H. Eisaki, J. Phys. Soc. Jpn. **81**, 104710 (2012).

[44] T. Kiss, T. Shimojima, K. Ishizaka, A. Chainani, T. Togashi, T. Kanai, X.-Y. Wang, C.-T. Chen, S. Watanabe, and S. Shin, Rev. Sci. Instrum. **79**, 023106 (2008).

[45] T. Yoshida, I. Nishi, S. Ideta, A. Fujimori, M. Kubota, K. Ono, S. Kasahara, T. Shibauchi, T. Terashima, Y. Matsuda, H. Ikeda, and R. Arita, Phys. Rev. Lett. **106**, 117001 (2011).

[46] T. Shimojima, F. Sakaguchi, K. Ishizaka, Y. Ishida, T. Kiss, M. Okawa, T. Togashi, C.-T. Chen, S. Watanabe, M. Arita, K. Shimada, H. Namatame, M. Taniguchi, K. Ohgushi, S. Kasahara, T. Terashima, T. Shibauchi, Y. Matsuda, A. Chainani, and S. Shin, Science **332**, 564 (2011).

[47] T. Shimojima, F. Sakaguchi, K. Ishizaka, Y. Ishida, W. Malaeb, T. Yoshida, S. Ideta, A. Fujimori, T. Kiss, M. Okawa, T. Togashi, C.-T. Chen, S. Watanabe, Y. Nakashima, A. Ino, H. Anzai, M. Arita, K. Shimada, H. Namatame, M. Taniguchi, S. Kasahara, T. Terashima, T. Shibauchi, Y. Matsuda, M. Nakajima, S. Uchida, K. Kihou, C. H. Lee, A. Iyo, H. Eisaki, A. Chainani, and S. Shin, Solid State Commun. **152**, 695 (2012).

[48] K. Suzuki, H. Usui, and K. Kuroki, J. Phys. Soc. Jpn. **80**, 013710 (2011).

[49] S. Hüfner, *Photoelectron Spectroscopy* (Springer, Berlin, 2003).

[50] R. S. Dhaka, S. E. Hahn, E. Razzoli, Rui Jiang, M. Shi, B. N. Harmon, A. Thaler, S. L. Bud'ko, P. C. Canfield, and A. Kaminski, Phys. Rev. Lett. **110**, 067002 (2013).

[51] V. Brouet, P.-H. Lin, Y. Texier, J. Bobroff, A. Taleb-Ibrahimi, P. Le Fèvre, F. Bertran, M. Casula, P. Werner, S. Biermann, F. Rullier-Albenque, A. Forget, and D. Colson, Phys. Rev. Lett. **110**, 167002 (2013).

[52] T. Yoshida, S. Ideta, T. Shimojima, W. Malaeb, K. Shinada, H. Suzuki, I. Nishi, A. Fujimori, K. Ishizaka, S. Shin, Y. Nakashima, H. Anzai, M. Arita, A. Ino, H. Namatame, M. Taniguchi, H. Kumigashira, K. Ono, S. Kasahara, T. Shibauchi, T. Terashima, Y. Matsuda, M. Nakajima, S. Uchida, Y. Tomioka, T. Ito, K. Kihou, C. H. Lee, A. Iyo, H. Eisaki, H. Ikeda, R. Arita, T. Saito, S. Onari, and H. Kontani, arXiv:1301.4818.

[53] Y. Nakai, T. Iye, S. Kitagawa, K. Ishida, H. Ikeda, S. Kasahara, H. Shishido, T. Shibauchi, Y. Matsuda, and T. Terashima, Phys. Rev. Lett. **105**, 107003 (2010).

[54] Y. Nakai, T. Iye, S. Kitagawa, K. Ishida, S. Kasahara, T. Shibauchi, Y. Matsuda, H. Ikeda, and T. Terashima, Phys. Rev. B **87**, 174507 (2013).

[55] Y. Nakashima, A. Ino, S. Nagato, H. Anzai, H. Iwasawa, Y. Utsumi, H. Sato, M. Arita, H. Namatame, M. Taniguchi, T. Oguchi, Y. Aiura, I. Hase, K. Kihou, C. H. Lee, A. Iyo, and H. Eisaki, Solid State Commun. **157**, 16 (2013).

[56] T. Terashima, N. Kurita, M. Tomita, K. Kihou, C. H. Lee, Y. Tomioka, T. Ito, A. Iyo, H. Eisaki, T. Liang, M. Nakajima, S. Ishida, S. I. Uchida, H. Harima, and S. Uji, Phys. Rev. Lett. **107**, 176402 (2011).

[57] Z. P. Yin, K. Haule, and G. Kotliar. Nature Physics, **7**, 294 (2011).

[58] M. Nakajima, S. Ishida, K. Kihou, Y. Tomioka, T. Ito, Y. Yoshida, C. H. Lee, H. Kito, A. Iyo, H. Eisaki, K. M. Kojima, and S. Uchida, Phys. Rev. B **81**, 104528 (2010).

[59] See supporting Online Material of Ref. 23 at http://www.sciencemag.org/content/329/5993/824/suppl/DC1.

[60] A. Damascelli, Z. Hussain, and Z. X. Shen, Rev. Mod. Phys. **75**, 473 (2003).

[61] V. Hinkov, D. Haug, B. Fauqué, P. Bourges, Y. Sidis, A. Ivanov, C. Bernhard, C. T. Lin, and B. Keimer, Science **319**, 597 (2008).

[62] M. J. Lawler, K. Fujita, J. Lee, A. R. Schmidt, Y. Kohsaka, C. K. Kim, H. Eisaki, S. Uchida, J. C. Davis, J. P. Sethna, and E.-A. Kim, Nature **466**, 347 (2010).

[63] R. M. Fernandes, A. V. Chubukov, J. Knolle, I. Eremin, and J. Schmalian, Phys. Rev. B **85**, 024534 (2012).

[64] R. M. Fernandes and J. Schmalian, Supercond. Sci. Technol. **25**, 084005 (2012).

[65] L. Zhang, P. F. Guan, D. L. Feng, X. H. Chen, S. S. Xie, and M. W. Chen, J. Am. Chem. Soc. **132**, 15223 (2010).

[66] J. J. Ying, X. F. Wang, T. Wu, Z. J. Xiang, R. H. Liu, Y. J. Yan, A. F. Wang, M. Zhang, G. J. Ye, P. Cheng, J. P. Hu, and X. H. Chen, Phys. Rev. Lett. **107**, 067001 (2011).

[67] E. C. Blomberg, M. A. Tanatar, R. M. Ferrnandes, I. I. Mazin, B. Shen, H.-H. Wen, M. D. Johannes, J. Schmalian, and R. Prozorov, Nature Communications **4**, 1914 (2013).

[68] S. Ishida, M. Nakajima, T. Liang, K. Kihou, C. H. Lee, A. Iyo, H. Eisaki, T. Kakeshita, Y. Tomioka, T. Ito, and S. Uchida, J. Am. Chem. Soc. **135**, 3158 (2013).